NANO LETTERS

pubs.acs.org/NanoLett Letter

Optical Bound States in Continuum in MoS_2-Based Metasurface for Directional Light Emission

Naseer Muhammad, Yang Chen, Cheng-Wei Qiu,* and Guo Ping Wang*

Cite This: *Nano Lett.* 2021, 21, 967−972 Read Online

ACCESS | Metrics & More | Article Recommendations | Supporting Information

ABSTRACT: High quality factor (*Q*-factor) and strong field localization in nanostructures is a newly emerged direction in nanophotonics. The bound states in the continuum (BIC) have been investigated in nanoparticles with infinite *Q*-factor. We report BIC in molybdenum disulfide (MoS_2) based Mie nanoresonator suspended in air. The ultrathin nanodisk supports symmetry protected BIC, and the quasi-BIC (*q*-BIC) are exploited by breaking the symmetry of the structure. The strongly localized modes in our MoS_2-based nanodisk sustain a similar magnetic field profile before and after symmetry breaking, unlike what has been previously reported in silicon-based structures. Strong directional emission is observed in BIC regime from a hybrid configuration with a resonator placed on the stacked metal-dielectric layers, which transform BIC to *q*-BIC and exploit highly directional light. The structure persists emission with small variations in normalized intensity at distorted symmetry. The giant *Q*-factor in *q*-BIC is highly desired for biosensing and optical filters.

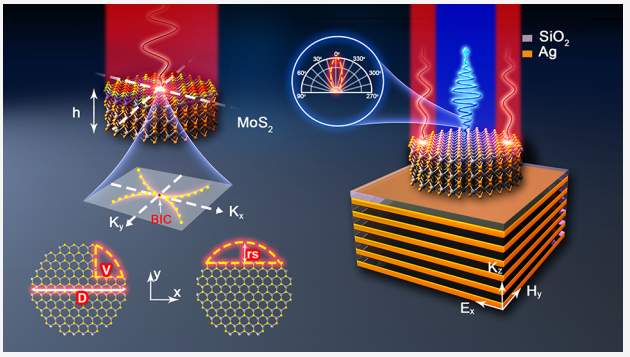

KEYWORDS: *hybrid metasurface, bound states, light emission, MoS_2, Q-factor, far field*

INTRODUCTION

Subwavelength structures arranged in two-dimensional arrays, so-called metasurfaces, have attracted enormous attention because of strong manipulation of light at nanoscale promising for applications in visible and infrared wavebands.[1−3] The dielectric metasurfaces have advantages over the plasmonic metasurfaces because of low dissipative losses in dielectric materials, which yield a high quality factor (*Q*-factor).[4,5] These advantages have been translated into well-pronounced optical features obtained in simple geometries compared to plasmonic metadevices for various applications including polarization and phase control,[6,7] sensing,[5] lenses,[8] and light emission.[9−11] The light emission efficiency is limited by dissipative losses of noble metals at optical frequencies.[12] The field enhancement at the metal surface due to the resonance condition can benefit the emission. However, because of high intrinsic losses, the fluorescence emitter at a certain point close to the metal surface results in a quenching problem, which can be deteriorating for the field emission.[13] On the other hand, a dielectric resonator in some cases can provide both electric and magnetic resonances, and in-phase oscillation of the resonance mode can produce a directional radiation.[12] Fluorescence nanoscopy use the nanoparticles bound to protein for illumination to detect and visualize the wanted region in subcellular structures.[14] The intrinsic protein fluorescence is too weak to reveal the detailed features and detection is a challenge at low concentration. For obtaining all-inclusive furtherance of efficiency, researchers have reported that the hybrid structure improves the fluorescence emission.[9,10] Sun et al. reported the highest directivity of just 3000 in a metal-dielectric hybrid structure with 74% power propagating in upward direction.[15] The main limitation in these hybrid and pure metal or dielectric structures is the weak localization of the incident field, which results in low emission intensity. Because of the unusual control of light in metasurfaces, perfectly confined modes, so-called bound states in continuum (BIC), have been investigated.[16] In principle, the *Q*-factor of these modes inclines to infinity and exists in the band of radiative modes with no leakage, which can be referred (occasionally) to embed trapped modes/eigenvalues.[16,17] However, in practical cases, the *Q*-factor is finite/reduced because of leakage into the substrate, material losses, fabrication imperfections, and roughness.[18,19] Different mechanisms have been used to perfectly localize modes such as symmetry protected or separability, tuning parameters (coupled resonances and single-resonance parametric BIC), and BICs from inverse construction (hopping rate, potential,

Received: September 21, 2020
Revised: January 8, 2021
Published: January 15, 2021

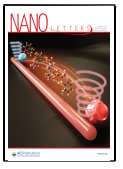

https://dx.doi.org/10.1021/acs.nanolett.0c03818
Nano Lett. 2021, 21, 967−972

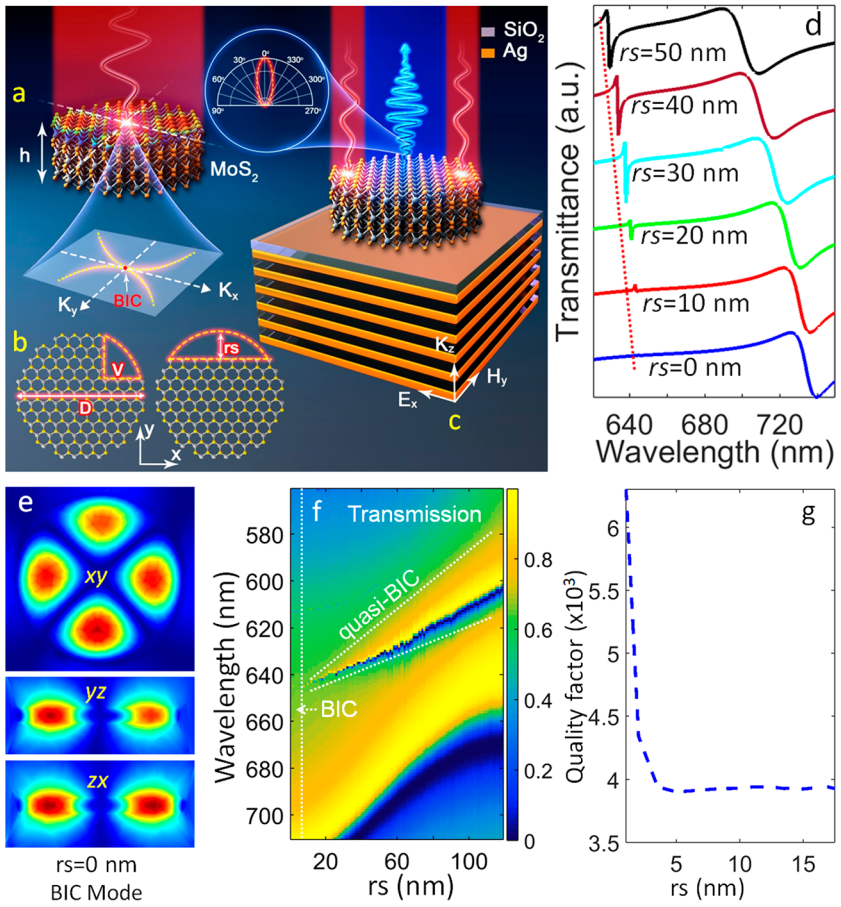

Figure 1. (a) Schematic of MoS_2 nanodisk; (b) top views of semispherical rs and V-edge cuts; (c) schematic of directional emission, thicknesses of SiO_2 and Ag are 21 and 21.5 nm, respectively; (d) transmission spectra; (e) magnetic field distribution around BIC at rs = 0 nm; (f) transmission spectra with respect to the rs values; and (g) *Q*-factor at different rs values.

and boundary shape engineering).[16] BICs have been explored for various applications such as directional lasing,[20,21] and image tuning.[19] BICs have also been exploited in various nanophotonics subwavelength resonators using silicon,[19,22] gallium arsenide,[20] indium gallium arsenide phosphide,[21] aluminum gallium arsenide,[23] hybrid structures,[24] and silicon nitride.[25] A noble metal is used as a resonator to achieve BIC modes, which results in a very small *Q*-factor (for practical case) due to dissipative losses.[26] Single-layer mechanically exfoliated transition metal dichalcogenides (TMDs) have been used on the top of the BIC structure to enhance the second-harmonic generation.[27] However, investigation of BICs in few-layer TMD-based metasurfaces remained elusive.

In this article, we employ a BIC-inspired Mie nanoresonator to design directional light routing using MoS_2, which can be fabricated as a radiative antenna recently reported in the literature.[28] The nanodisk possesses a symmetry-protected BIC, and quasi-BIC (*q*-BIC) is exploited by cutting the semispherical and V-edge of the cylinder to reduce the symmetry of the structure. The *Q*-factor is inclined to infinity at zero size of cuts, and it decreases as the cuts sizes are increased. The modes are strongly localized and sustainable in the MoS_2-based resonator, which is distinct from the observation of mode-changing fashion in thicker Si nanodisks.[19] The highest normalized intensities are calculated at the wavelengths around BIC in nanodisks on the dielectric-metal stack, making a hybrid structure of TMD-dielectric-metal. The highest far-field intensity in this work is above 73 900, which is many fold higher than previously reported. The structure maintains the emission after introducing cuts in the resonator or around *q*-BICs, which confirms emission from a BIC-inspired structure.

METHODS AND MATERIALS

We consider a square unit cell consists of an ultrathin nanodisk made of MoS_2 as a Mie resonator structure (Figure S1). In two-dimensional (2D) materials, molybdenum disulfide (MoS_2: indirect to direct bandgap when shrink to monolayers) in particular, is more promising because of the excellent tunability with variations in number of layers for optoelectronic applications at nanoscale.[29,30] On the contrary, TMDs can be fabricated in a single step as dielectric radiative antennas due to high refractive index in visible and part of infrared.[28] The multilayer MoS_2 has superiorities over conventional semiconductors such as Si because of its high refractive index and the face it has no losses/absorption in infrared[31] and over the monolayer because of its higher optical density of state and strong photon absorption capability.[32] Coulomb interaction is innate in monolayer MoS_2 and comparatively stronger than the quasi-two-dimensional common dielectric because of the high effective mass of MoS_2.[29] The Coulomb interactions in multilayer TMDs result in strong binding energy of the excitons and the TMD radiative decay time (τ_r^{ex}) is two orders of magnitude shorter than GaAs-quantum wells[33] in magnitude $\left(\frac{1}{2\Gamma_{ex}} \lesssim 1\text{ps}\right)$, which can be written with

https://dx.doi.org/10.1021/acs.nanolett.0c03818
Nano Lett. 2021, 21, 967−972

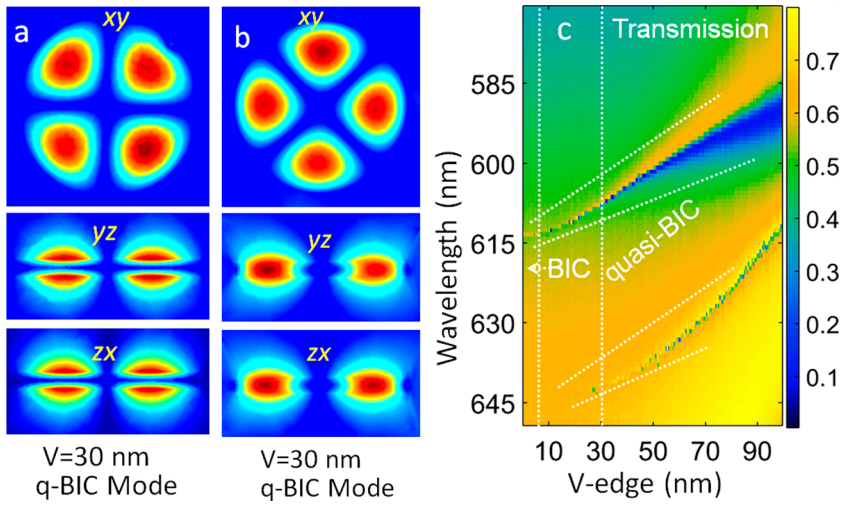

Figure 2. Magnetic field distribution of q-BIC around (a) 611 nm at V = 30 nm, (b) 640 nm at V = 30 nm, and (c) transmission spectra with respect to the V values.

expression:[34,35] $\tau_r^{ex} = \frac{1}{2\Gamma_{ex}} = \frac{\hbar\varepsilon}{2k_{ex}}\left(\frac{E_{X^{ex}}}{e\hbar v}\right)^2 (r_B^{2d})^2$, where Γ_{ex} represents the radiative decay, k_{ex} is the light wave-vector, $E_X$ex is excitation energy, and r_B^{2d} is exciton Bohr radius. The expression of light-wave vector is $k_{ex} = E_{X^{ex}}\sqrt{\varepsilon}/\hbar c$ where ε is dielectric constant, c is speed of light, and v is Kane velocity. The Bohr radius can be calculated using the formula: $(r_B^{2d}) = (E\hbar^2)/(4\mu_{ex}e^2)$, where μ_{ex} with reduced exciton mass is $1/\mu_{ex} = 1/m_{ee} + 1/m_{hh}$, where m_{ee} and m_{hh} are the effective mass of electron and hole, respectively.

The emission in TMDs is affected by excitons and trions because of the reduced dielectric screening and Coulomb interaction in small dimensionality.[33,36] The excitation energy of A and B excitation bands as a function of temperature (T) described by semiempirical formula based on electron−phonon interaction[37,38] is $E_X(T) = E_X$ex $- S\langle\hbar w\rangle[\coth((\langle\hbar w\rangle/(2k_BT)) - 1]$, where $\langle\hbar w\rangle$ is average phonon energy contributing to the change in T of the $E_X$ex, S is effective electron−phonon coupling constant, and k_B is Boltzmann constant. The trion photoluminescence intensity[38] is given as $I(\hbar w) = exp[(-E_{tr}^0 - \hbar w)/\varepsilon]\Theta\ (E_{tr}^0 - \hbar w)/\varepsilon$, where $1/\varepsilon = (m_{ee}/m_X)(1/(k_BT) + (m_X/m_{tr})(4\ m_{ee}a^2)/\hbar^2)$, E_{tr}^0 is zero-momentum trion energy, Θ is the unit step function, and m_X, m_{tr} are the mass of exciton and trion, respectively. In silicon the optical transition is indirect, dependent on the surface structure, photoluminescence arises from quantum electronic states, and quite low at very thin geometry down to few nanometers.[39] The dielectric constant in conventional materials is controlled by band structures. Conversely, in MoS_2, luminescence behavior originates from allowed direct electronic transitions and thus results in a high recombination rate.[40] The dielectric constant of MoS_2 is in sharp contrast with common dielectric materials and dominated by the tightly bound excitons. It decreases when the number of layers increases from single to five layers, but after five or seven layers, it increases along with the thickness of the film.[41] The dependence of the dielectric function can be written in simplified expression as[41] $\varepsilon_2(\omega) = A_0J_{cv}|U(0)|^2$, where A_0 represents all the terms, which are independent of number of layers, J_{cv} is the joint density of states (valence and conduction band) involved in the transition, 0 is the electron-holes physical overlap wave function, U is the relative motion wave function of holes and electrons via Coulomb interactions, and $|U(0)|^2$ excitonic effect on oscillator strength of the interband transition.

The two-dimensional metasurface array is generated by applying Floquet boundary conditions which repeat the unit-cell infinitely in both x- and y-direction. Perfect matched layer is applied at both ports in the z-direction to circumvent the boundary reflections.[26] The dimensions of the structure are: each side length of unit-cell is p = 470 nm, diameter of the ultrathin nanodisk is D = 380 nm, thickness h = 36 nm, rs is the semispherical edge, and V represents the size of V-edge. The x-polarized plane-wave beam carrying unit-power[7] is applied with 0° incident angle propagating in the z-direction. The dielectric constant of MoS_2 is taken from the experimental data[28] and the simulation space is filled with air $(n = 1)$. Comsol Multiphysics is used for all simulations throughout the article.

RESULTS AND DISCUSSIONS

We first consider the resonator suspended in air composed of MoS_2 nanodisk carefully engineered as shown in Figure 1a. The nanodisk supports symmetry protected BIC at gamma point where both x- and y-components of emission wave-vectors are zero $(k_x = k_y = 0)$.[20,42] Due to zero net radiation the BIC does not manifest itself in the transmission spectra as shown in Figure 1d (blue curve). To reveal the immersion of BIC in nanodisk we cut edge rs of disk to reduce the geometric symmetry[43] and open channel for outgoing power[19] as shown in Figure 1b. It can be seen from the transmission spectra (red curve) in Figure 1d a small split appears around 639 nm due to the interaction of the mode energy with free space. The radiation loss grows as the radius of the cut edge increases; this is due to large numbers of open radiation channels.

To see the mechanism of bound states, we calculated the magnetic field distribution (in the xy-plane profile, the state has diagonal nodal planes) at the corresponding wavelength as shown in Figure 1e at rs = 0 nm, and the modes are strongly confined inside the nanodisk without energy exchange between the localized mode and the free space. The magnetic field distributions at the resonant point of the transmission spectra at rs = 50 nm (q-BIC) are calculated (Figure S2c Supporting Information). At reduced symmetry the trapped modes are still

https://dx.doi.org/10.1021/acs.nanolett.0c03818
Nano Lett. 2021, 21, 967−972

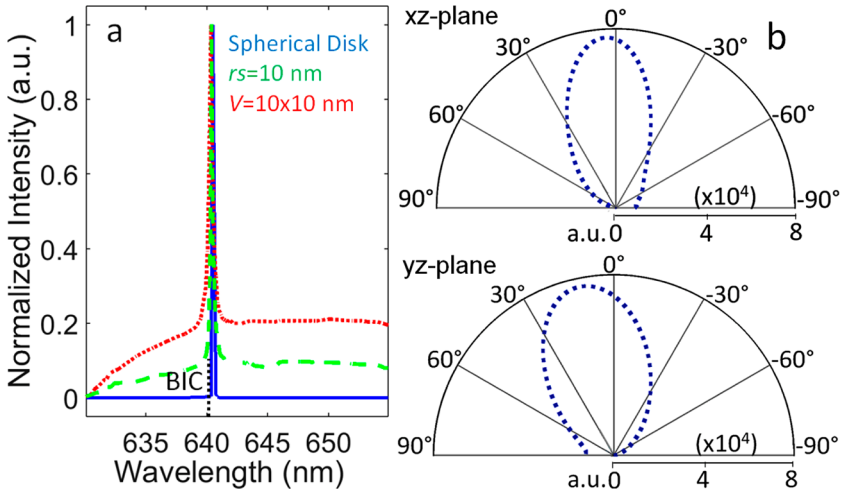

Figure 3. (a) Normalized intensity of emission from the nanodisk around BIC (rs/V = 0 nm), rs = 10 nm, and V = 10 × 10 nm; (b) pattern of light emission intensity at the corresponding wavelength in the *xz*-plane and *yz*-plane.

strongly localized which can be used for boosting light-matter interactions. Figure 1f shows the calculated transmission spectra from 0 nm cut-edge to around 120 nm a narrow split emerges around 5 nm and become broad as the cut-edge approaches higher values. We calculated the *Q*-factor using the expression $Q = \lambda/\Delta\lambda$, where λ is the corresponding wavelength and $\Delta\lambda$ represents the full-width half-maximum. At 0 nm cut-edge the line-width is zero, the applied field is perfectly confined, featuring infinite *Q*-factor and lifetime.

Figure 1g shows that the *Q*-factor decreases for small rs cut-edge as we introduce symmetry breaking. Although, the drop in *Q*-factor is small for the cut-edge rs >10 nm due to the reason that the BIC is transformed to a leaky resonance mode and there is no further significant increase in number of radiation channels and thus result in small variation in *Q*-factor for rs >10 nm (and estimated from eigenfrequencies the *Q*-factor decreases with increase in cut-edge shown in Figure S3a). Through this transformation of BIC can be tuned to *q*-BIC, to manifest itself in the transmission spectra with certain spectral width of the resonance and thus the *Q*-factor. So, it can be said that one can engineer the desired *Q*-factor using the transformation of BIC to *q*-BIC in subwavelength structures-on-demand wanted for numerous applications. Further, we cut a V-edge from the same nanodisk to transform BIC to *q*-BIC as shown in Figure 1b. To see the physical mechanism of the trapped modes, we calculated a magnetic field profile for *q*-BIC at the corresponding wavelengths. It can be seen in Figure 2a, b that magnetic modes are strongly localized in all three components (*xy*, *yz*, *zx*) at V = 30 nm around 611 nm (in *xy*-plane profile, the state has nodal planes along x and y) and 640 nm (in the *xy*-plane profile, the state has diagonal nodal planes similar to Figure 1e), respectively. Furthermore, the transmission spectrum is calculated with respect to an increase in the size of the V-edge. As the cut size increases from small values to 100 nm the spectral width of the split in transmission spectra increases as shown in Figure 2c. This is because the radiation grows with an increase in the size of the V-edge, which results in a resonance with broad spectral width analogous to the Fano line-shape. The appearance of *q*-BIC mode and the same magnetic field profile at V = 30 nm in Figure 2b support the confirmation of BIC at around 640 nm as investigated in the previous case with introducing a semispherical edge cut. We calculated the *Q*-factor for both modes; the *Q*-factor of the mode around 611 nm is high (decline is small) up to V = 15 nm (Figure S3). However, the *Q*-factor decreases as we incorporate the V-edge cut in the nanodisk for the mode around 640 nm. It can be said that the BIC-inspired mechanism provides a route to achieving the desired *Q*-factor by judiciously engineering the metasurface. BIC modes have been reported previously in a Si nanodisk with a thickness of 53 nm and a period of 840 nm.[19]

Compared to that work, our MoS_2-based structure maintains the magnetic modes similarly before and after symmetry breaking. This is due to the fact that the dielectric function of few-layer TMDs are dominated by tightly bound exciton unlike dependent on the band structures as in common dielectric materials. In TMD-based structures, the optical features arise from the hybridization of excitons and optical modes,[28] whereas in common dielectric, such features are supported by geometrical optical modes. Also, our general mechanism demonstrates similarly well-pronounced mode profiles in both symmetry-breaking cases, as illustrated in Figure 1b.

To demonstrate the light emission from our BIC-inspired TMDs metasurface, the nanodisk is placed on the stack of metal-dielectric layers, as shown in Figure 1c. A pair of six layers made of silicon dioxide (SiO2: Ghosh 1999) and silver (Ag: Johnson and Christy data) acted as a cavity. In our design, the stacking contributes to the transition of nonradiative BIC to radiative mode (Figure S4),[18] decreases the *Q*-factor, and exploits the emission around BIC wavelength. A strong emission is observed at wavelength around BIC at spherical disk on stack without any cut as shown in Figure 3a (blue curve). The normalized values of intensity around BIC wavelengths show that the light emission is much higher comparing to the rest of waveband. The radiated field in the direction of strong emission and field propagation in one-direction are basic properties to characterize the device which can be observed from Figure 3b. The far-field intensity at corresponding wavelength as high as >73 900 (directional intensity normalized to the free space is I/I_0 = 33 590, where I is the total intensity and I_0 is intensity in free space[15] (Figure S5), and maximum power is directed in one direction.[44] This is due to the structure perfectly localizing the incident field and generating astonishing electromagnetic field a few orders higher than the incident field. The collaborative effect of the excitons and optical modes in the TMD-dielectric-metal hybrid

https://dx.doi.org/10.1021/acs.nanolett.0c03818
Nano Lett. 2021, 21, 967−972

structure teaming up is the outstanding directional routing performance compared to their pure, dielectric-metal, and other counterparts.[9−11,15,20,45] The strong directional emission can be used to enhance the efficiency of fluorescence nanoscopy and fluorescence sensing.

To confirm the robustness of emission from BIC-inspired structure, we placed the nanodisk with an rs = 10 nm cut on the stack. The emission persists around the corresponding wavelength. The rs = 10 nm cut breaks the symmetry of the structure and has open energy exchange with the free space, resulting in low photoluminescence, which can be observed from the comparison of the green curve with the blue curve in Figure 3a. This is due to the fact that in the full nanodisk case, the resonator confines the strong field (as it supports BIC in the suspended-in-air case, although the dielectric-metal cavity distorts the BIC by leaky losses to the stack (Figure S4) and transforms it to *q*-BIC and decreases the *Q*-factor), which couples it to the cavity and results in strong photoluminescence. However, in the rs = 10 nm cut case (the resonator supports *q*-BIC, which is not perfectly confined in the suspended-in-air case), the mode coupling to the cavity is weak compared to the full resonator, and thus results in comparatively low photoluminescence. Further, we place the nanodisk with a V-edge cut of $V = 10 \times 10$ nm, a small variation can be seen in the line-width of the normalized intensity curve around *q*-BIC at other wavelengths. It is worth noting that symmetry breaking has no significant effect on the emission intensity. In the device design and fabrication process, this is of great importance to reduce the impact on emission from trapped modes.

CONCLUSION

In this letter, we report perfect trapped modes in MoS_2-based metasurface suspended in air. The ultrathin nanodisk supports symmetry-protected BIC, and the *q*-BICs are achieved by introducing cuts in the structure. Well-pronounced and perfectly trapped modes are achieved in our MoS_2-based nanostructure. Strong directional emission is seen around BIC when transformed to radiative mode by placing it on the stack of metal-dielectric layers as a light-emitting diode. The emission remains around *q*-BIC with small changes in normalized intensity after breaking the symmetry. The emission efficiency and directional intensity is higher than previously reported hybrid structures. The *q*-BICs in our work can also be used to design high *Q*-factor devices for optical filtering, biosensing, and slow-wave photonics. To our knowledge we present this hybrid combination for the first time, which combines the coupling of excitons and optical modes in the same structure will strengthen the traditional nanophotonics with potential applications.

ASSOCIATED CONTENT

Supporting Information

The Supporting Information is available free of charge at https://pubs.acs.org/doi/10.1021/acs.nanolett.0c03818.

Simulation method and setting; *Q*-factor estimated from eigen-frequencies; *Q*-factor and field distribution; *Q*-factor calculated for different *V* values; magnetic field profile (leaky modes) of nanodisk on metal-dielectric stack; emission intensity, emission intensity normalized to the free space, and normalized intensity (standardized form) (PDF)

AUTHOR INFORMATION

Corresponding Authors

Cheng-Wei Qiu − *Department of Electrical and Computer Engineering, National University of Singapore, Singapore 117583, Singapore;* orcid.org/0000-0002-6605-500X; Email: chengwei.qiu@nus.edu.sg

Guo Ping Wang − *Institute of Microscale Optoelectronics, Shenzhen University, Shenzhen 518060, China;* Email: gpwang@szu.edu.cn

Authors

Naseer Muhammad − *Institute of Microscale Optoelectronics, Shenzhen University, Shenzhen 518060, China; Department of Electrical and Computer Engineering, National University of Singapore, Singapore 117583, Singapore;* orcid.org/0000-0002-7290-280X

Yang Chen − *Department of Electrical and Computer Engineering, National University of Singapore, Singapore 117583, Singapore;* orcid.org/0000-0002-8501-5417

Complete contact information is available at: https://pubs.acs.org/10.1021/acs.nanolett.0c03818

Notes

The authors declare no competing financial interest.

ACKNOWLEDGMENTS

This work is supported by the NSFC (Grants 11734012 and 12074267), and Science & Technology Project of Guangdong (2020B010190001). C.-W.Q. acknowledges the support from the National Research Foundation, Prime Minister's Office, Singapore, under its Competitive Research Programme (CRP award NRF CRP22-2019-0006). C.W.Q. is also supported by a grant (R-261-518-004-720) from Advanced Research and Technology Innovation Centre (ARTIC).

REFERENCES

(1) Overvig, A. C.; Shrestha, S.; Malek, S. C.; Lu, M.; Stein, A.; Zheng, C.; Yu, N. Dielectric metasurfaces for complete and independent control of the optical amplitude and phase. *Light: Sci. Appl.* **2019**, *8* (1), 92.

(2) Shafiei, F.; Monticone, F.; Le, K. Q.; Liu, X.-X.; Hartsfield, T.; Alù, A.; Li, X. A subwavelength plasmonic metamolecule exhibiting magnetic-based optical Fano resonance. *Nat. Nanotechnol.* **2013**, *8* (2), 95.

(3) Liu, J.; Li, Z.; Liu, W.; Cheng, H.; Chen, S.; Tian, J. High-Efficiency Mutual Dual-Band Asymmetric Transmission of Circularly Polarized Waves with Few-Layer Anisotropic Metasurfaces. *Adv. Opt. Mater.* **2016**, *4* (12), 2028−2034.

(4) Miroshnichenko, A. E.; Kivshar, Y. S. Fano resonances in all-dielectric oligomers. *Nano Lett.* **2012**, *12* (12), 6459−6463.

(5) Yang, Y.; Kravchenko, I. I.; Briggs, D. P.; Valentine, J. All-dielectric metasurface analogue of electromagnetically induced transparency. *Nat. Commun.* **2014**, *5*, 5753.

(6) Chen, G.; Wen, Z.-Q.; Qiu, C.-W. Superoscillation: from physics to optical applications. *Light: Sci. Appl.* **2019**, *8* (1), 56.

(7) Khaidarov, E.; Liu, Z.; Paniagua-Dominguez, R.; Ha, S. T.; Valuckas, V.; Liang, X.; Akimov, Y.; Bai, P.; Png, C. E.; Demir, H. V.; Kuznetsov, A. I. Control of LED Emission with Functional Dielectric Metasurfaces. *Laser Photonics Rev.* **2020**, *14* (1), 1900235.

(8) Liu, W.; Li, Z.; Cheng, H.; Tang, C.; Li, J.; Zhang, S.; Chen, S.; Tian, J. Metasurface Enabled Wide-Angle Fourier Lens. *Adv. Mater.* **2018**, *30* (23), 1706368.

(9) Shibanuma, T.; Grinblat, G.; Albella, P.; Maier, S. A. Efficient third harmonic generation from metal-dielectric hybrid nanoantennas. *Nano Lett.* **2017**, *17* (4), 2647−2651.

(10) Liu, J.-N.; Huang, Q.; Liu, K.-K.; Singamaneni, S.; Cunningham, B. T. Nanoantenna-Microcavity Hybrids with Highly Cooperative Plasmonic-Photonic Coupling. *Nano Lett.* **2017**, *17* (12), 7569−7577.
(11) Feng, T.; Zhang, W.; Liang, Z.; Xu, Y.; Miroshnichenko, A. E. Isotropic magnetic Purcell effect. *ACS Photonics* **2018**, *5* (3), 678−683.
(12) Krasnok, A. E.; Miroshnichenko, A. E.; Belov, P. A.; Kivshar, Y. S. All-dielectric optical nanoantennas. *Opt. Express* **2012**, *20* (18), 20599−20604.
(13) Wu, W.; Shi, N.; Zhang, J.; Wu, X.; Wang, T.; Yang, L.; Yang, R.; Ou, C.; Xue, W.; Feng, X.; et al. Electrospun fluorescent sensors for the selective detection of nitro explosive vapors and trace water. *J. Mater. Chem. A* **2018**, *6* (38), 18543−18550.
(14) Li, C.; Kuang, C.; Liu, X. Prospects for fluorescence nanoscopy. *ACS Nano* **2018**, *12* (5), 4081−4085.
(15) Sun, S.; Zhang, T.; Liu, Q.; Ma, L.; Du, Q.; Duan, H. Enhanced directional fluorescence emission of randomly oriented emitters via a metal-dielectric hybrid nanoantenna. *J. Phys. Chem. C* **2019**, *123* (34), 21150−21160.
(16) Hsu, C. W.; Zhen, B.; Stone, A. D.; Joannopoulos, J. D.; Soljačić, M. Bound states in the continuum. *Nature Reviews Materials* **2016**, *1* (9), 16048.
(17) Bulgakov, E. N.; Sadreev, A. F. Bound states in the continuum in photonic waveguides inspired by defects. *Phys. Rev. B: Condens. Matter Mater. Phys.* **2008**, *78* (7), 075105.
(18) Sadrieva, Z. F.; Sinev, I. S.; Koshelev, K. L.; Samusev, A.; Iorsh, I. V.; Takayama, O.; Malureanu, R.; Bogdanov, A. A.; Lavrinenko, A. V. Transition from optical bound states in the continuum to leaky resonances: role of substrate and roughness. *ACS Photonics* **2017**, *4* (4), 723−727.
(19) Xu, L.; Zangeneh Kamali, K.; Huang, L.; Rahmani, M.; Smirnov, A.; Camacho-Morales, R.; Ma, Y.; Zhang, G.; Woolley, M.; Neshev, D.; Miroshnichenko, A. E. Dynamic Nonlinear Image Tuning through Magnetic Dipole Quasi-BIC Ultrathin Resonators. *Advanced Science* **2019**, *6* (15), 1802119.
(20) Ha, S. T.; Fu, Y. H.; Emani, N. K.; Pan, Z.; Bakker, R. M.; Paniagua-Domínguez, R.; Kuznetsov, A. I. Directional lasing in resonant semiconductor nanoantenna arrays. *Nat. Nanotechnol.* **2018**, *13* (11), 1042−1047.
(21) Kodigala, A.; Lepetit, T.; Gu, Q.; Bahari, B.; Fainman, Y.; Kanté, B. Lasing action from photonic bound states in continuum. *Nature* **2017**, *541* (7636), 196.
(22) Koshelev, K.; Lepeshov, S.; Liu, M.; Bogdanov, A.; Kivshar, Y. Asymmetric metasurfaces with high-Q resonances governed by bound states in the continuum. *Phys. Rev. Lett.* **2018**, *121* (19), 193903.
(23) Carletti, L.; Koshelev, K.; De Angelis, C.; Kivshar, Y. Giant nonlinear response at the nanoscale driven by bound states in the continuum. *Phys. Rev. Lett.* **2018**, *121* (3), 033903.
(24) Azzam, S. I.; Shalaev, V. M.; Boltasseva, A.; Kildishev, A. V. Formation of bound states in the continuum in hybrid plasmonic-photonic systems. *Phys. Rev. Lett.* **2018**, *121* (25), 253901.
(25) Yang, Y.; Peng, C.; Liang, Y.; Li, Z.; Noda, S. Analytical perspective for bound states in the continuum in photonic crystal slabs. *Phys. Rev. Lett.* **2014**, *113* (3), 037401.
(26) Liang, Y.; Koshelev, K.; Zhang, F.; Lin, H.; Lin, S.; Wu, J.; Jia, B.; Kivshar, Y. Bound states in the continuum in anisotropic plasmonic metasurfaces. *Nano Lett.* **2020**, *20* (9), 6351−6356.
(27) Bernhardt, N.; Koshelev, K.; White, S. J.; Meng, K. W. C.; Froch, J. E.; Kim, S.; Tran, T. T.; Choi, D.-Y.; Kivshar, Y.; Solntsev, A. S. Quasi-BIC resonant enhancement of second-harmonic generation in WS2 monolayers. *Nano Lett.* **2020**, *20* (7), 5309−5314.
(28) Verre, R.; Baranov, D. G.; Munkhbat, B.; Cuadra, J.; Käll, M.; Shegai, T. Transition metal dichalcogenide nanodisks as high-index dielectric Mie nanoresonators. *Nat. Nanotechnol.* **2019**, *14* (7), 679−683.
(29) Radisavljevic, B.; Kis, A. Mobility engineering and a metal-insulator transition in monolayer MoS 2. *Nat. Mater.* **2013**, *12* (9), 815−820.
(30) Mak, K. F.; Shan, J. Photonics and optoelectronics of 2D semiconductor transition metal dichalcogenides. *Nat. Photonics* **2016**, *10* (4), 216.
(31) Ermolaev, G. A.; Stebunov, Y. V.; Vyshnevyy, A. A.; Tatarkin, D. E.; Yakubovsky, D. I.; Novikov, S. M.; Baranov, D. G.; Shegai, T.; Nikitin, A. Y.; Arsenin, A. V. Broadband optical properties of monolayer and bulk MoS 2. *npj 2D Materials and Applications* **2020**, *4*, 21.
(32) Li, Y.; Xu, H.; Liu, W.; Yang, G.; Shi, J.; Liu, Z.; Liu, X.; Wang, Z.; Tang, Q.; Liu, Y. Enhancement of exciton emission from multilayer MoS2 at high temperatures: intervalley transfer versus interlayer decoupling. *Small* **2017**, *13* (17), 1700157.
(33) Reeves, L.; Wang, Y.; Krauss, T. F. 2D material microcavity light emitters: to lase or not to lase? *Adv. Opt. Mater.* **2018**, *6* (19), 1800272.
(34) Palummo, M.; Bernardi, M.; Grossman, J. C. Exciton radiative lifetimes in two-dimensional transition metal dichalcogenides. *Nano Lett.* **2015**, *15* (5), 2794−2800.
(35) Robert, C.; Lagarde, D.; Cadiz, F.; Wang, G.; Lassagne, B.; Amand, T.; Balocchi, A.; Renucci, P.; Tongay, S.; Urbaszek, B.; Marie, X. Exciton radiative lifetime in transition metal dichalcogenide monolayers. *Phys. Rev. B: Condens. Matter Mater. Phys.* **2016**, *93* (20), 205423.
(36) Wang, G.; Chernikov, A.; Glazov, M. M.; Heinz, T. F.; Marie, X.; Amand, T.; Urbaszek, B. Colloquium: Excitons in atomically thin transition metal dichalcogenides. *Rev. Mod. Phys.* **2018**, *90* (2), 021001.
(37) Tongay, S.; Zhou, J.; Ataca, C.; Lo, K.; Matthews, T. S.; Li, J.; Grossman, J. C.; Wu, J. Thermally driven crossover from indirect toward direct bandgap in 2D semiconductors: MoSe2 versus MoS2. *Nano Lett.* **2012**, *12* (11), 5576−5580.
(38) Christopher, J. W.; Goldberg, B. B.; Swan, A. K. Long tailed trions in monolayer MoS 2: Temperature dependent asymmetry and resulting red-shift of trion photoluminescence spectra. *Sci. Rep.* **2017**, *7* (1), 1−8.
(39) Godefroo, S.; Hayne, M.; Jivanescu, M.; Stesmans, A.; Zacharias, M.; Lebedev, O.; Van Tendeloo, G.; Moshchalkov, V. V. Classification and control of the origin of photoluminescence from Si nanocrystals. *Nat. Nanotechnol.* **2008**, *3* (3), 174.
(40) Splendiani, A.; Sun, L.; Zhang, Y.; Li, T.; Kim, J.; Chim, C.-Y.; Galli, G.; Wang, F. Emerging Photoluminescence in Monolayer MoS2. *Nano Lett.* **2010**, *10* (4), 1271−1275.
(41) Yu, Y.; Yu, Y.; Cai, Y.; Li, W.; Gurarslan, A.; Peelaers, H.; Aspnes, D. E.; Van de Walle, C. G.; Nguyen, N. V.; Zhang, Y.-W.; Cao, L. Exciton-dominated dielectric function of atomically thin MoS 2 films. *Sci. Rep.* **2015**, *5*, 16996.
(42) Zhen, B.; Hsu, C. W.; Lu, L.; Stone, A. D.; Soljačić, M. Topological nature of optical bound states in the continuum. *Phys. Rev. Lett.* **2014**, *113* (25), 257401.
(43) Campione, S.; Liu, S.; Basilio, L. I.; Warne, L. K.; Langston, W. L.; Luk, T. S.; Wendt, J. R.; Reno, J. L.; Keeler, G. A.; Brener, I.; Sinclair, M. B. Broken symmetry dielectric resonators for high quality factor Fano metasurfaces. *ACS Photonics* **2016**, *3* (12), 2362−2367.
(44) Curto, A. G.; Volpe, G.; Taminiau, T. H.; Kreuzer, M. P.; Quidant, R.; van Hulst, N. F. Unidirectional Emission of a Quantum Dot Coupled to a Nanoantenna. *Science* **2010**, *329* (5994), 930−933.
(45) Harats, M. G.; Livneh, N.; Rapaport, R. Design, fabrication and characterization of a hybrid metal-dielectric nanoantenna with a single nanocrystal for directional single photon emission. *Opt. Mater. Express* **2017**, *7* (3), 834−843.

https://dx.doi.org/10.1021/acs.nanolett.0c03818
Nano Lett. 2021, 21, 967−972